



Research Article

## Determination of the breast cancer tumor diameter using a UWB microwave antenna system

Çetin KURNAZ<sup>1,\*</sup>, Fawzy ALSHARIF<sup>1</sup>, Adnan Ahmad CHEEMA<sup>2</sup>

<sup>1</sup>Department of Electrical and Electronic Engineering, Ondokuz Mayıs University, Samsun, 55139, Türkiye

<sup>2</sup>SenComm Research Lab, School of Engineering, Ulster University, Jordanstown, BT1 6DN, United Kingdom

### ARTICLE INFO

#### Article history

Received: 07 September 2021

Revised: 13 November 2021

Accepted: 26 November 2021

#### Keywords:

Ultra-Wideband Antenna;  
Breast Cancer; Tumor Detection;  
Microwave Imaging

### ABSTRACT

This paper presents a novel ultra-wideband microwave antenna system to detect breast cancer and estimate tumor diameter. The system operates within the frequency range of 1 to 12 GHz and comprises a microstrip-fed monopole antenna that encircles the breast to identify the presence of tumors. The study demonstrates that a tumor within the breast can be detected by observing changes in the distribution of current density within the breast tissue, particularly in regions containing tumors of varying sizes. The research findings reveal that the system can identify breast tumors with the highest recorded current density of 188 A/m<sup>2</sup> in cases with a tumor diameter of 30 mm, while the lowest recorded current density is 140 A/m<sup>2</sup> for tumors with a diameter of 5 mm. Furthermore, the highest Specific Absorption Rate (SAR) value measured at the surface of the breast model is 0.2 W/kg. To determine the diameter of the tumors, the system collects and analyzes backscattered waves from a breast model. The investigation covers tumors with diameters ranging from 1 mm to 35 mm, and the received signals are recorded. In contrast to prior research, this study introduces an empirical model with a remarkable accuracy rate of 92.28% for characterizing the diameter of breast tumors based on the measurement analysis.

**Cite this article as:** Kurnaz Ç, Alsharif F, Cheema AA. Determination of the breast cancer tumor diameter using a UWB microwave antenna system. Sigma J Eng Nat Sci 2023;41(5):999–1012.

### INTRODUCTION

Breast cancer is a prevalent health concern among women, ranking as the most common cancer type and second overall worldwide [1]. In 2018, there were over 2 million new cases of breast cancer globally, a number projected to surpass 3 million by 2040 [3]. In the United States, approximately 1 in 8 women is at risk of developing breast cancer during her lifetime, with an estimated 276,480 new

cases expected in 2020 [4]. Similarly, about 1 in 8 European women may experience breast cancer before age 85 [5]. The early detection of breast cancer is crucial for identifying and halting the progression of malignant tissue. Early diagnosis significantly enhances the chances of successful treatment, with a five-year survival rate exceeding 90% [6,7]. Consequently, regular screening plays a pivotal role in early detection. Traditional methods such as magnetic resonance

#### \*Corresponding author.

\*E-mail address: ckurnaz@omu.edu.tr; cetin.kurnaz@gmail.com

This paper was recommended for publication in revised form by  
Regional Editor Ahmet Selim Dalkılıç



imaging (MRI), ultrasound, and X-ray mammography have been the standard approaches for breast cancer screening. However, X-ray mammography is associated with a limited detection rate, and many women report discomfort during the examination [8-11]. In the case of ultrasound, the quality of diagnosis depends on the operator's ability, while the reproducibility of results is very poor [12-14]. The MRI is a more effective and susceptible technique and is quick to detect the tumor than mammography. However, it is costly and has significantly high false positive test results [15]. Recently, microwave imaging in detecting breast cancer has become an attractive interest [16-21], with differentiation between fibroglandular tissue and cancerous tissue based on the differences in the scatter of the microwaves produced by different tissues [22, 23]. The utilization of microwave imaging for breast cancer detection presents a promising and cost-effective alternative [24]. In an ultra-wideband (UWB) microwave imaging system, low-power pulses are emitted by a transmitter antenna, after which a receiver antenna captures the scattered signals to facilitate breast cancer detection [25, 26]. For effective microwave imaging, it is imperative that the antenna used be planar and possess high radiation efficiency across the entire frequency range of interest [27]. However, it's worth noting that many wide-band antennas typically exhibit omnidirectional radiation characteristics and tend to have lower efficiency [28, 29]. The antenna types like circular [30-32], Vivaldi [33, 34], and Bowtie [35] have been widely used in such applications. A wearable antenna is one of the standard test subjects for body-driven correspondence. A wearable antenna is a part of the clothing used for correspondence purposes, and it allows continuous health monitoring of the patient, especially with a high risk for cancer. In addition, wearable antenna devices for all new applications must be lightweight, inexpensive, almost fix-free, and have no foundation [36].

Microwave imaging has emerged as an active field of research, with various antenna designs proposed for breast cancer detection in the existing literature. For instance, Sharma et al. [37] developed a UWB antenna sensor probe, operating within the frequency range of 2.8 GHz to 20 GHz, specifically designed to detect malignant breast cells. Their analysis incorporated parameters such as the magnitude and phase of reflection and the Specific Absorption Rate (SAR). Islam et al. [38] introduced a comprehensive breast phantom measurement system featuring the Vivaldi antenna with a bandwidth spanning approximately 1.54 GHz to 7 GHz. This system was devised for phantom breast measurements, facilitating the detection of tumor cells within the breast. An automated electromechanical imaging system was also proposed as part of their work. Zhang [39] presented a radar-based microwave imaging system for breast cancer detection. Their approach relied on a complex natural response method to differentiate between benign and malignant tumors, with high dielectric differences between the tumor and surrounding tissues playing a pivotal role

in determining tumor location. Successful discrimination was achieved even between benign spherical tumors with a radius of 5 mm and malignant tumors with an average radius of 5 mm. Kwon et al. [40] proposed a time-domain microwave breast imaging system, incorporating Gaussian bandpass filtering and conducting comprehensive analyses. Subramanian et al. [41] employed a modified octagonal-shaped ultra-wideband monopole microstrip antenna constructed with FR4 material for breast cancer detection. The antenna operated across a frequency range from 3 GHz to 15 GHz, and SAR was utilized to identify malignant tissue within a three-dimensional breast model with a radius of 60 mm. Misilmani et al. [42] explored different array configurations based on antenna parameters for microwave breast imaging. Hammouch and Ammor [43] designed and optimized a UWB antenna to achieve a favorable impedance match within the specified frequency range of 3.1 GHz to 14 GHz. They also introduced a confocal microwave imaging algorithm to detect and locate tumors by analyzing various electromagnetic signals. Rahayu et al. [44] devised circular and rectangular antenna arrays in a ring configuration, operating within the frequency range of 2 GHz to 11 GHz, for breast tumor detection. Alsharif and Kurnaz [45] employed parameters such as E-Field, H-Field, and SAR to ascertain the presence of tumors (e.g.,  $r = 4$  mm) within the breast. They further proposed an ultra-wideband (UWB) microwave antenna system for early breast cancer detection, even in cases involving multiple tumors. Alsharif and Kurnaz [46] evaluated various microstrip patch antennas, including Vivaldi, Bowtie, circular patch, and rectangular patch microstrip antennas, commonly used in microwave imaging. Their assessment considered size, radiation patterns, efficiency, and wearability, ultimately revealing that rectangular wearable antennas exhibited wider bandwidths and higher radiation efficiencies. Lastly, Alsharif and Kurnaz [47] proposed an improved bandwidth microstrip antenna tailored for ultra-wideband breast cancer detection. Simulation experiments conducted in CST software involved the collection of backscattered waves from a breast phantom model.

The literature encompasses three primary methods for detecting tumor cells within the breast in the context of microwave imaging systems. The initial approach involves utilizing electric field (E), magnetic field (H), and current density values within the malignant breast. The second method relies on Specific Absorption Rate (SAR) to identify the presence of a tumor. In contrast, the third method capitalizes on signals obtained from the reflection of the breast, with or without a tumor. This study adopts all three distinct approaches to discern breast cancer tumors. Notably, in contrast to previous investigations, the central aim of this study is to leverage a UWB microwave antenna system for the dual purposes of breast cancer detection and the estimation of tumor diameter.

Firstly, a wearable microstrip antenna operated at frequencies 1 GHz - 12 GHz was designed and manufactured

to achieve these goals. In this study, a wearable microstrip antenna was used because it has wider bandwidth and higher radiation efficiency [46], and the operating frequency range from 1 GHz to 12 GHz was chosen since the conductivity and permittivity of normal and malignant breast tissue vary significantly in this frequency range [14, 48]. The antenna parameters, such as reflection coefficient, radiation patterns, total efficiency, and directivity, were obtained. Also, the antenna's reflection coefficient under different bending conditions was analyzed. Secondly, using CST software, a breast model was created, replicating the physical properties of a human breast, and within this model, a tumor was incorporated. This designed breast model comprises three distinct layers. These include a hemispherical skin layer, 3 mm thick and 50 mm in diameter, fibro glandular bosom greasy cells, and a defective tumor. Current density with various tumor sizes and SAR distribution of the breast model were investigated. Finally, the breast model was placed in front of the transmitter and receiver antennas, and the breast model's backscattered waves with a tumor diameter range of 1 mm to 35 mm were recorded. To determine the diameter of the breast tumor, a novel empirical model was proposed using receive signals. Compared to previous studies, this study provides the following key contributions: Firstly, a microstrip patch is used to apply the wearable antenna application by using pure cotton as a substrate of the proposed antenna, as it can be made conformal for integration into clothing.

Human bodies are different from one another. Identifying the components in the tissues that need to be considered for antenna design is essential. The movement of body parts will also reduce antenna performance. We cannot restrict movement; therefore, we need to identify which body part is less affected by activity. Furthermore, the designed antenna was tested under two bending modes to show its performance. The antenna designed for breast cancer detection works with safety standards, SAR values less than the safety limit, and the proposed antenna model achieved it. Even though the antenna structure can be patch type, textile, or implanted antenna, the priority is to achieve the best performance during its operation. Power consumption, bandwidth, throughput, and safety must be considered during the design. The review gives a brief idea for new researchers on the current structure of an on-body implanted antenna based on different objectives and purposes. Cancer detection is easily affected by environmental factors such as temporal physical obstructions. The signal can be degraded due to interference from another wireless device. This can prevent the data from being efficiently transmitted and reduce the device's reliability and energy efficiency. It becomes more challenging when the human body can also distort the signal. These factors must be addressed to ensure the antenna bandwidth and throughput can be optimally designed—finally, the antenna form factor and the user's safety. Besides being physically safe, it must also be safe regarding E.M. wave and heat dissipation

during operation. The user must be comfortable when using the device.

## PREPARATION OF ANTENNA DESIGN AND PERFORMANCE MEASUREMENTS

A breast cancer tumor comprises various cell types within the breast, each exhibiting distinct genetic profiles, growth rates, and metastatic potential. Importantly, the electrical properties of malignant breast tissues deviate significantly from those of healthy breast tissues across the microwave frequency spectrum [49, 50]. In this context, a UWB microwave antenna system can identify tumors by capitalizing on the contrasting dielectric constants between normal and malignant tissues. To accomplish this, transceiver antennas strategically positioned around the breast play a pivotal role in capturing the backscattered signals emanating from the breast tissue. These received signals are subsequently employed to detect the presence of malignant tissues within the breast. The antennas used for microwave imaging must possess key attributes such as high gain, broad bandwidth, and increased directionality to probe deeper-seated tumors within the breast effectively.

The dimensions of the antenna are calculated by equations (1), (2), (3), and (4), where  $L$  and  $W$  represent the length and width of the antenna [51]. The patch width of the antenna is calculated using equations (1) [51, 52],

$$W = \frac{c}{2f_r} \sqrt{\frac{2}{\epsilon_r + 1}} \quad (1)$$

Here,  $c$  represents the speed of light,  $f_r$  denotes the resonance frequency, and  $\epsilon_r$  signifies the relative permittivity.

The effective dielectric constant is calculated using equation (2), where  $h$  is the substrate thickness [53].

$$\epsilon_{\text{eff}} = \frac{\epsilon_r + 1}{2} + \frac{\epsilon_r - 1}{2} \left[ 1 + 12 \frac{h}{W} \right]^{-\frac{1}{2}} \quad (2)$$

The extension length of the antenna is obtained using equation (3) [54].

$$\Delta L = 0.412 h \frac{(\epsilon_{\text{eff}} + 0.3) \left( \frac{W}{h} + 0.264 \right)}{(\epsilon_{\text{eff}} - 0.258) \left( \frac{W}{h} + 0.8 \right)} \quad (3)$$

The antenna length is obtained using equation (4) [55].

$$L = \frac{c}{2f_r \sqrt{\epsilon_{\text{eff}}}} - 2\Delta L \quad (4)$$

The ground-plane width and length of the antenna can be obtained as given in equations (5) and (6).

$$W_s = W + 6h \quad (5)$$

$$L_s = L + 6h \tag{6}$$

Creating a small slot extending in the same direction as the feed line on the ground plane was essential to enhance the operational bandwidth. The antenna's substrate measures 70 mm x 60 mm, with a relative permittivity of 1.6 and a thickness of 1.6 mm. For constructing both the patch and ground planes, a flexible copper material with a thickness of 0.1 mm was employed. Figure 1 provides a visual representation of the geometric dimensions of the ground and patch planes.

The antenna is connected via a 50 Ω small-scale (SMA) connector. As mentioned earlier, the components of this antenna were acquired from references [54, 55] and modeled using CST Microwave Studio [56]. In the fabrication process, pure cotton was employed to enhance the substrate's wearability, along with polyester copper. Additionally, an

SMA connector was utilized for the feed. Figure 2 provides both front and rear views of the proposed antenna.

The antenna's geometric configuration was modeled and analyzed using CST Microwave Studio, and the physically constructed design was subjected to testing using the PNA Network Analyzer (Keysight N9951A, capable of measuring frequencies up to 44 GHz) for evaluating the antenna's reflection coefficient.

**Reflection Coefficient**

The designed antenna operates within a frequency range from 1 GHz to 12 GHz. It exhibits a -10 dB reflection coefficient ( $S_{11}$ ) bandwidth extending up to 9.6 GHz, as shown in Figure 3.

**Bending of Antenna**

The wearable antenna is designed to flex in response to human body movements and must maintain consistent

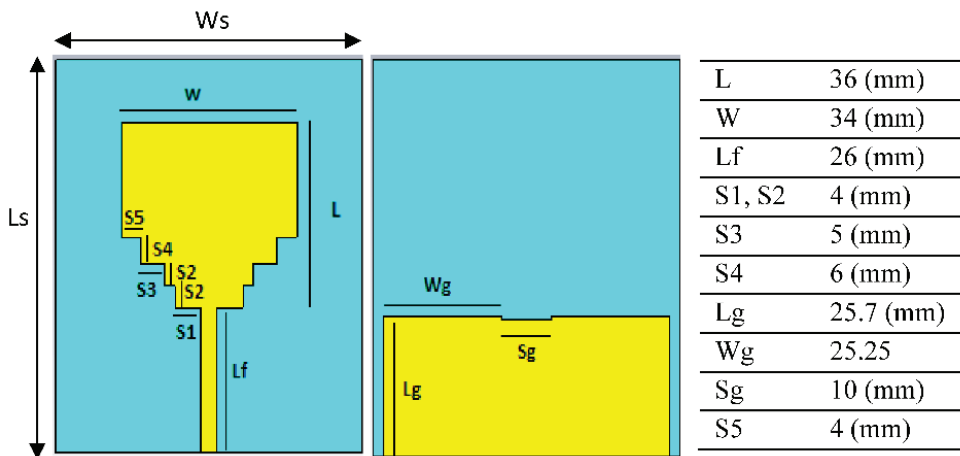


Figure 1. Dimensions of the proposed antenna.

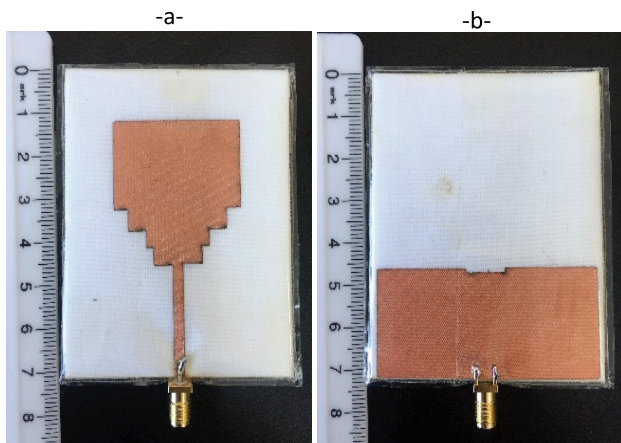


Figure 2. Prototype of the proposed antenna: a) front view, b) back view.

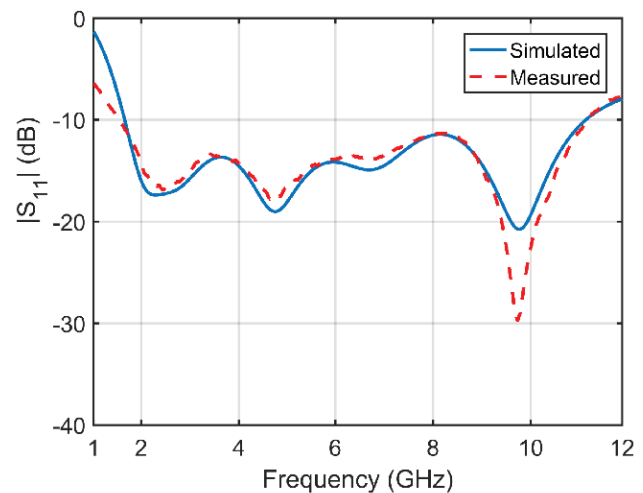
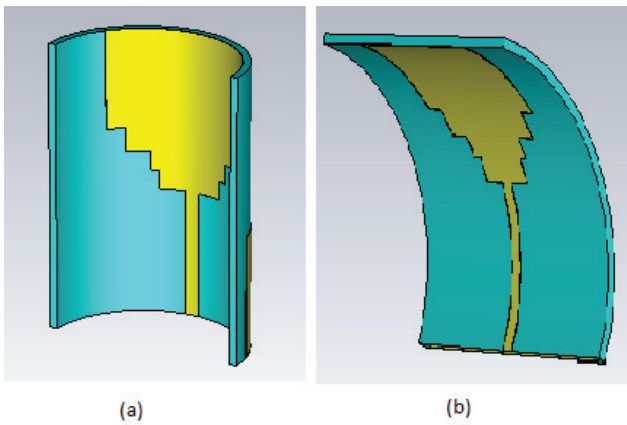


Figure 3. Reflection coefficient for both the simulated and measured antenna.



**Figure 4.** Simulated antenna bending using two distinct modes: a) vertical and b) horizontal bending.

performance across various body locations. The proposed antenna underwent testing under diverse conditions to assess its expected operational bandwidth. The antenna was subjected to bending in different vertical and horizontal orientations at a 45-degree angle, as depicted in Figure 4.

As depicted in Figure 5, the  $S_{11}$  value of the antenna remains consistently within the ultra-wide bandwidth range under various bending conditions, including both horizontal and vertical orientations. This indicates the antenna's ability to function effectively under these bending conditions.

**Radiation Pattern**

An anechoic chamber was employed to measure the antenna's radiation patterns in the E-plane, as depicted in Figure 6. Figure 7 illustrates the polar representation of the radiation patterns in free space at different frequencies (2.5 GHz, 5.8 GHz, 6.8 GHz, and 9.8 GHz) when the substrate

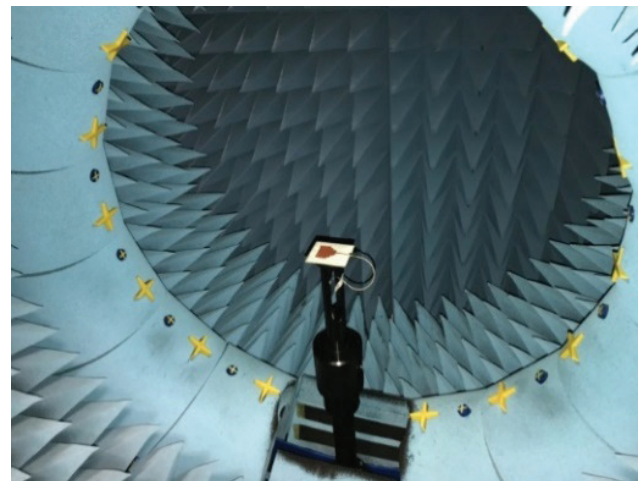


**Figure 6.** Measurement of antenna's radiation patterns.

is constructed from pure cotton, and the patch and ground planes are composed of polyester copper, maintaining their purity.

Figure 8 presents the comprehensive simulated efficiency of the antenna. As depicted, the antenna maintains a total efficiency exceeding 90% across the entire frequency band from 1.6 GHz to 11.2 GHz. The antenna exhibits a directional radiation pattern directed towards the broadside, achieving a peak gain of 6.76 dBi at 9.8 GHz, as illustrated in Figure 9.

**BREAST MODEL**

The proposed breast model, which includes a simulated tumor, closely mimics the physical properties of the human breast. This model has three distinct layers, as referenced in [45]. The first layer represents the skin, forming a semi-sphere

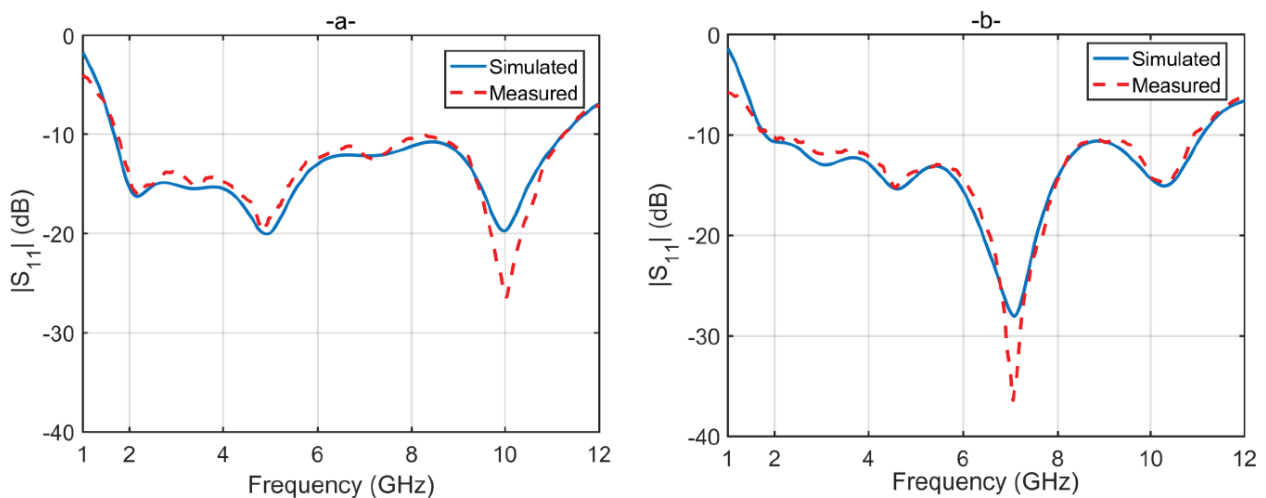


**Figure 5.** The  $S_{11}$  value of the designed antenna is assessed for a) vertical and b) horizontal bending.

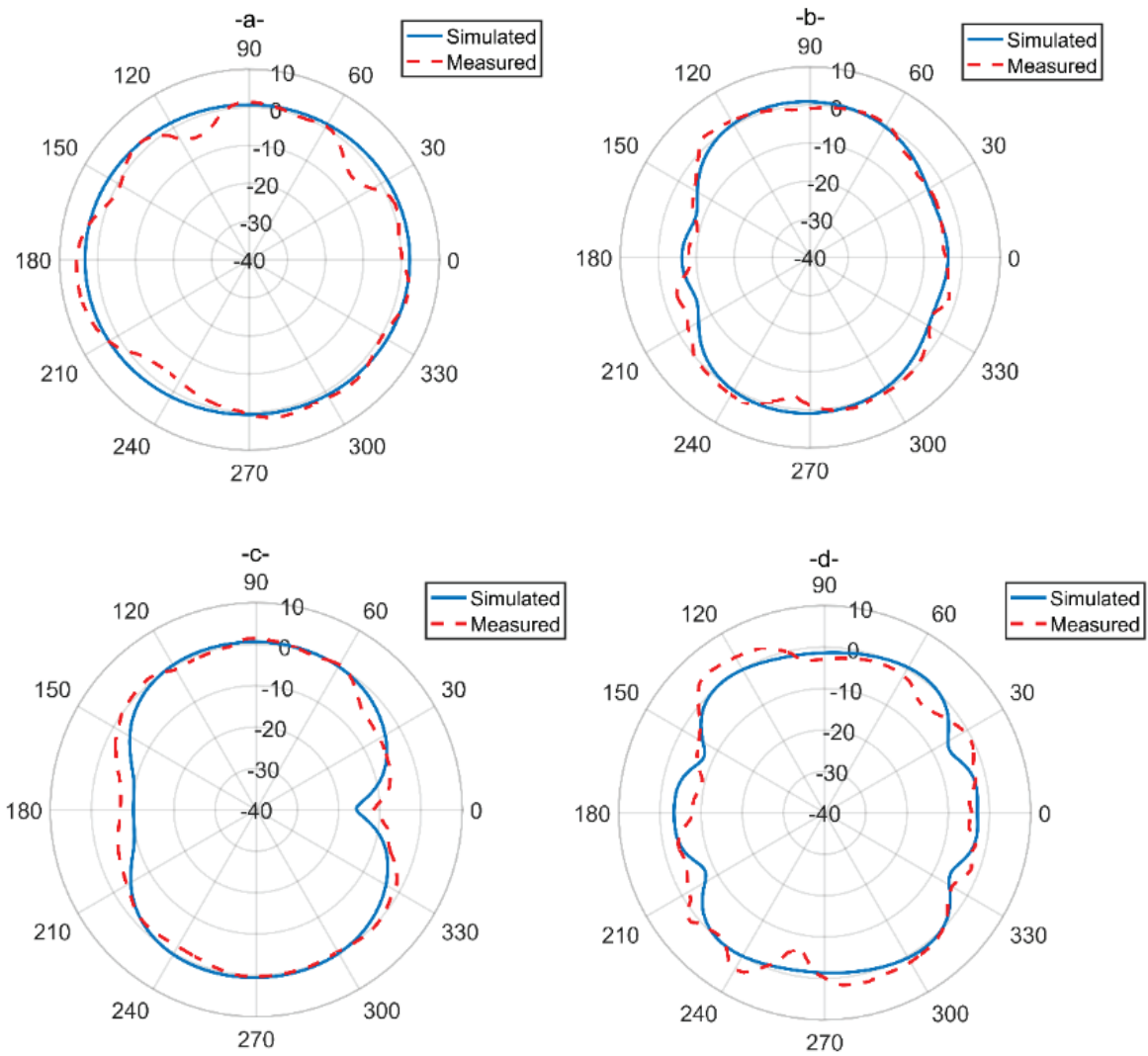


Figure 7. Antenna’s radiation pattern at a) 2.5 GHz, b) 5.8 GHz, c) 6.8 GHz, d) 9.8 GHz.

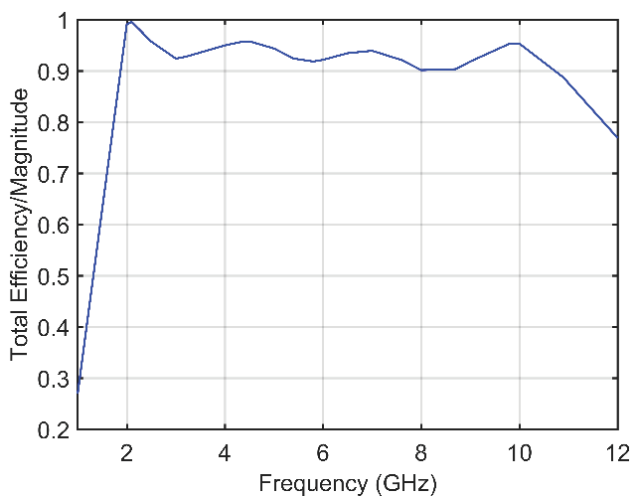


Figure 8. The total simulated efficiency of the antenna.

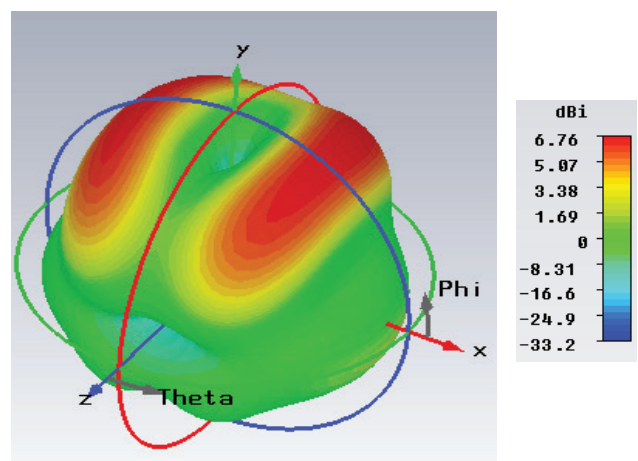


Figure 9. Directivity of the antenna at 9.8 GHz.

**Table 1.** Physical properties of each layer in the breast model

Medium	Relative Permittivity	Conductivity [S/m]
Skin	46.7	1.1
Normal cell	9	0.15
Defected (Tumor) cell	50	0.7

**Table 2.** The current density of tumors with various diameters

Tumor diameter [mm]	Current density [A/m <sup>2</sup> ]
5	140
10	160
15	165
20	180
25	185
30	188

with a thickness of 3 mm and a diameter of 50 mm. The second layer encompasses fibro glandular breast tissue and fatty cells, forming another semi-sphere within the skin layer with an outer radius of 22 mm. Within this fibro glandular layer, a defective tumor (representing glandular tissue) is positioned as a sphere, with a variable diameter ranging from 5 mm to 30 mm. Table 1 provides the specific physical properties of each layer within the breast model [57]. Given that signals interact with and scatter off the current density of objects, tumors of various sizes (ranging from 5 mm to 30 mm) were

incorporated into the model to assess breast cancer detection. Figure 10 visually illustrates the current density distribution around the tumor’s surface.

Table 2 presents current density estimations for tumors at different measurements. The current density within the tumor ranges from 140 A/m<sup>2</sup> to 188 A/m<sup>2</sup>, with higher

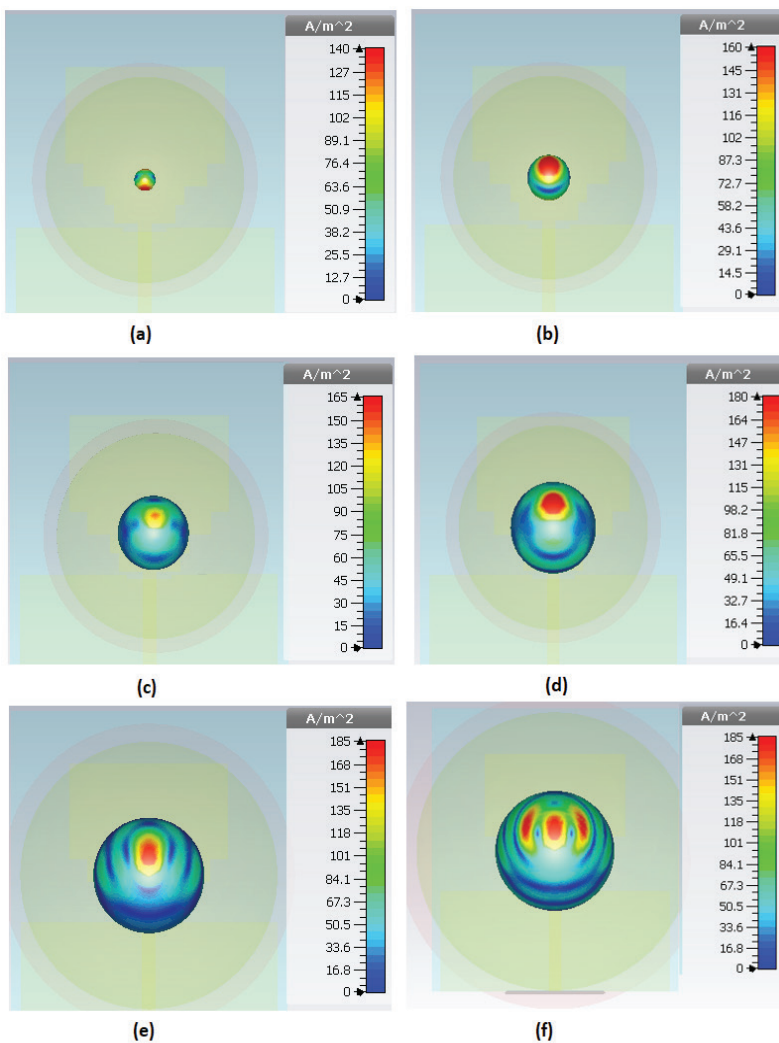


**Figure 10.** The simulated current density of the breast with various tumor sizes: a) 5 mm, b) 10 mm, c) 15 mm, d) 20 mm, e) 25 mm, f) 30 mm.

values indicating enhanced disease detectability. As demonstrated by the simulation results, the antenna's sensitivity to tumor presence or its ability to detect anomalies is heightened when the receiving antenna makes contact with the skin of the breast.

The SAR encompasses a range of frequencies from 1.6 GHz to 11.2 GHz. This SAR analysis was conducted using CST software, employing the IEEE Std. C95.3-2002 averaging method [58] with a tissue volume exceeding 10 grams. The ICNIRP standard imposes a limit of 2 W/kg, averaging

over 10 grams of tissue [59]. Figure 11 illustrates the SAR distribution within the phantom when a wearable antenna is placed adjacent, maintaining a 5 mm separation. The highest SAR value recorded is 0.2 W/kg at the phantom's surface, deemed acceptable for detection purposes under a transmitting power level of 200 mW and with a 5 mm separation between the antennas and the breast model. It's important to note that higher SAR values within the distribution can potentially harm and damage breast tissue. The focal area of SAR changes as the frequency shifts from lower

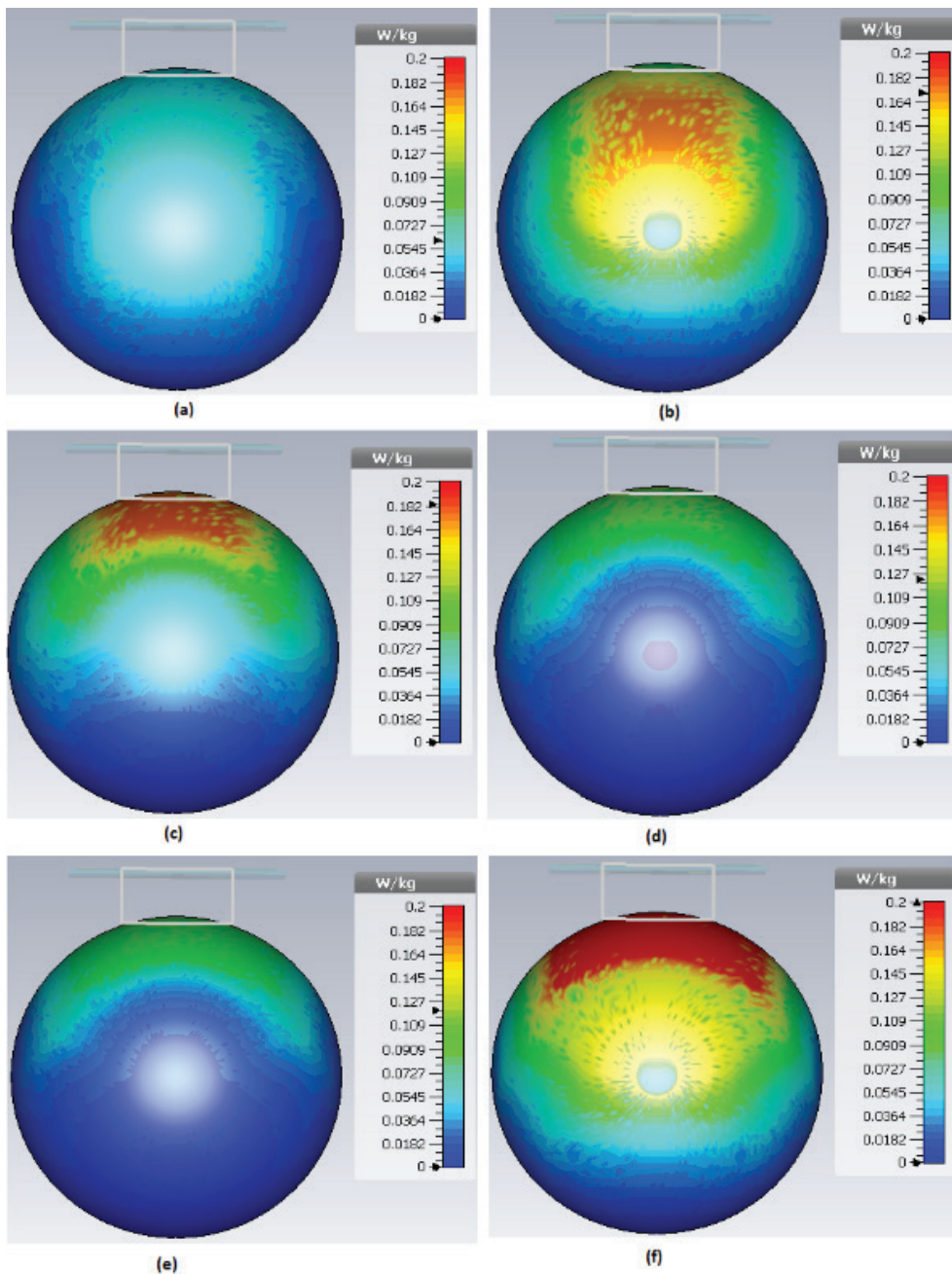


**Figure 11.** Distribution of SAR within the breast model phantom at various frequencies: a) 1 GHz, b) 2.5 GHz, c) 5.8 GHz, d) 6.8 GHz, e) 7.1 GHz, and f) 9.8 GHz.

to higher ranges. Higher frequencies can detect deeply situated small-sized tumors due to their shorter wavelengths. In comparison, lower frequencies are employed for detecting deeply established medium and large-sized tumors due to their longer wavelengths. The designed antenna operates effectively within the frequency range of 1.6 GHz to 11.2 GHz, delivering a uniform SAR distribution deep within the phantom.

### TUMOR DETECTION

The phantom breast model is positioned in front of the transmitter and receiver antennas, forming a 180-degree angle with a bending configuration, as illustrated in Figure 12 [45, 47]. Throughout the simulations conducted in

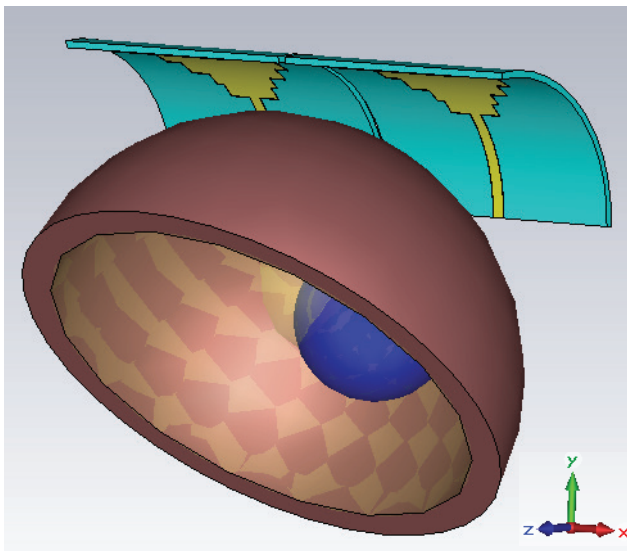


Figure 12. Breast model with tumor and (Tx, Rx) antennas.

this study, it is assumed that there is no mutual coupling between the antennas, and the surrounding environment remains constant. The behavior of the tumor was analyzed over a time interval ranging from 0.5 to 0.75 nanoseconds while varying the tumor's diameter within the range of 1 to 35 mm within the breast model. Figure 13 displays the signal transmitted to the breast model, and Figure 14 (a) illustrates the received signal from the breast model with and without a tumor. The synchronization steps are based on factors such as heartbeat and skin scattering characteristics [57, 60]. As evident from Figure 14 (b), alterations in the diameter of the tumor within the breast model result in changes in the amplitude of the received signal. When the tumor size increases, the time shift decreases while the amplitude increases. This indicates that larger tumors can reflect signals more rapidly than smaller ones. Variations in the amplitude and arrival time of the received signal can be

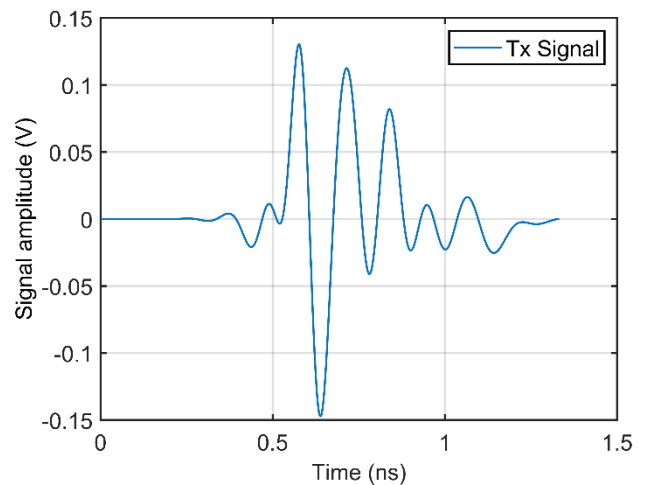


Figure 13. Transmitted signal.

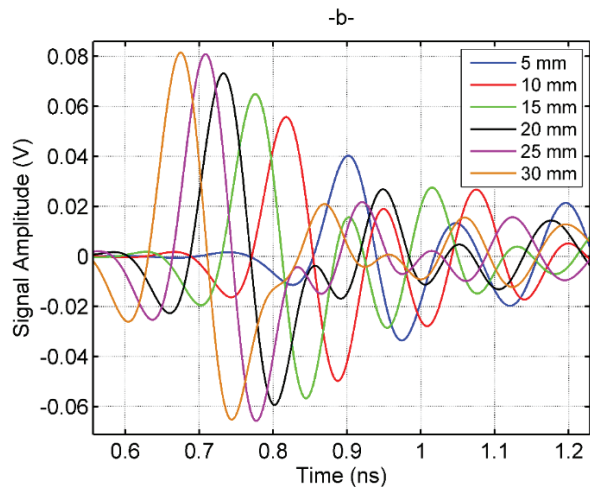
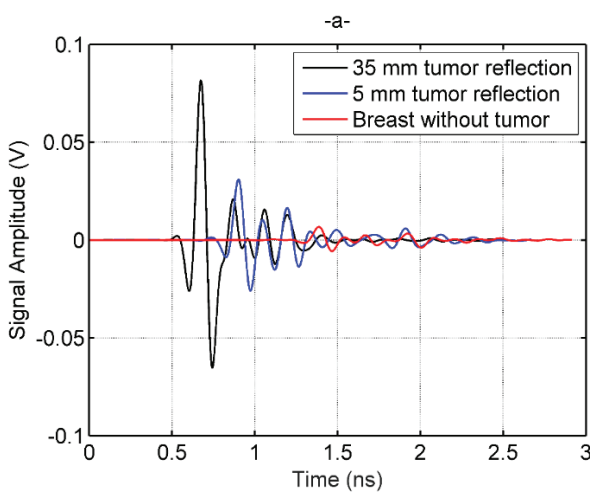


Figure 14. Received signal corresponding to tumor behavior: a) Breast with and without a tumor, and b) Responses for tumors of varying diameters.

attributed to multipath propagation and differing distances between the tumor and the antenna.

A Multiple Linear Regression (MLR) approach is employed to ascertain the breast tumor's diameter to analyze the received signals. In the MLR model, the dependent variable is correlated with a minimum of two independent variables, as expressed below:

$$D_n = \beta_0 + \beta_1 A_{n1} + \beta_2 T_{n1} + \dots + \beta_{k-1} A_{Nk} + \beta_k T_{Nk} + \varepsilon_n, n = 1, 2, \dots, N \quad (7)$$

Where  $D_n$  represents the tumor diameter,  $\beta$  denotes the regression coefficients,  $A$  stands for amplitude, and  $T$  represents time, as illustrated in Figure 11.  $N$  represents the size of the dataset,  $\varepsilon_n$  represents errors, and  $k$  indicates the number of variables. Equation (7) can be expressed in matrix form, as presented in equation (8).

$$D = X\beta + \varepsilon; \begin{bmatrix} D_1 \\ D_2 \\ \vdots \\ D_N \end{bmatrix} = \begin{bmatrix} 1 & A_{11}T_{11} & \dots & A_{1k-1}T_{1k} \\ 1 & A_{21}T_{21} & \dots & A_{2k-1}T_{21} \\ \vdots & \vdots & \ddots & \vdots \\ 1 & A_{N1}T_{N1} & \dots & A_{Nk-1}T_{Nk} \end{bmatrix} \begin{bmatrix} \beta_0 \\ \beta_1 \\ \vdots \\ \beta_k \end{bmatrix} + \begin{bmatrix} \varepsilon_1 \\ \varepsilon_2 \\ \vdots \\ \varepsilon_N \end{bmatrix} \quad (8)$$

The regression coefficients can be calculated as follows [64]:

$$\hat{\beta} = (X^T X)^{-1} X^T D \quad (9)$$

The method's precision is evaluated using the Normalized Root Mean Squared Error (NRMSE), defined in equation (10).

$$\text{NRMSE} = \frac{\sqrt{\frac{1}{N} \sum_{n=1}^N (D_n - \hat{D}_n)^2}}{\max(D_n) - \min(D_n)} \quad (10)$$

In this equation,  $D_n$  represents the actual tumor diameter,  $\hat{D}_n$  is the estimated  $D_n$  value,  $n$  is the index number, and  $N$  is the total data.

In this study, determining breast tumor diameter involved utilizing a dataset comprising 25 different diameter values, ranging from 1 mm to 35 mm. 18 were allocated for model training, and the remaining 7 were designated for model testing. This division into training and testing datasets was carried out to mitigate the impact of data variations and gain a deeper understanding of the model's characteristics. The training dataset was employed to construct a regression model, while the test (or validation) dataset was utilized to validate the model's performance. The regression coefficients of the model were derived from equation (7) using the training data. The estimation model for tumor diameter was developed based on the amplitudes and time interval values of the received signal (denoted as  $A_{in}$  and  $T_{in}$ ), as depicted in Figure 15. Specifically, when utilizing only the amplitude  $A_{i1}$ , the diameter estimation was accomplished using equation (11). In this scenario, the NRMSE values for training and testing were found to be 0.1202 and 0.1527, respectively.

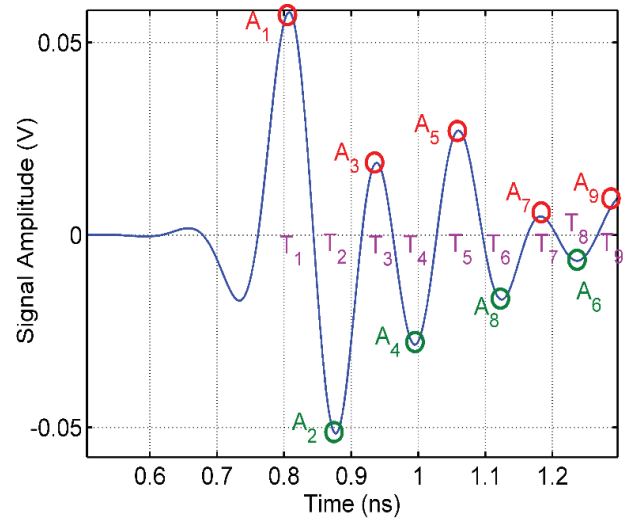


**Figure 15.** Amplitudes and time intervals of the received signal.

By incorporating both  $A_{i1}$  and  $T_{i1}$ , the diameter estimation was achieved using equation (12). Under these conditions, the NRMSE values for training and testing were determined to be 0.1099 and 0.1350, respectively. When  $A_{i1}$ ,  $T_{i1}$ ,  $A_{i2}$ , and  $T_{i2}$  were considered, the diameter estimation was conducted using equation (13). In this configuration, the NRMSE values for training and testing were 0.061 and 0.0989, respectively. Furthermore, when the variables  $A_{i1}$ ,  $T_{i1}$ ,  $A_{i2}$ ,  $T_{i2}$ ,  $A_{i3}$ ,  $T_{i3}$ ,  $A_{i4}$ , and  $T_{i4}$  were all considered, the diameter estimation was performed using equation (14). In this particular scenario, the NRMSE values for training and testing were determined to be 0.0443 and 0.0865, respectively.

$$\hat{D}_n = -13 + 484,1 A_{n1} \quad (11)$$

$$\hat{D}_n = -44,2 + 670,9 A_{n1} + 23,6 T_{n1} \quad (12)$$

$$\hat{D}_n = -66,8 + 1603,7 A_{n1} - 496,3 T_{n1} + 11185,4 A_{n2} + 508,2 T_{n2} \quad (13)$$

$$\hat{D}_n = -34,8 + 2222,9 A_{n1} + 1594,9 T_{n1} + 1359 A_{n2} - 1532,8 T_{n2} - 20 A_{n3} - 491,1 T_{n3} - 170,2 A_{n4} + 501,9 T_{n4} \quad (14)$$

The best outcomes and related techniques are given in equation (15) for curtness.

$$\hat{D}_n = -105,6 + 1975,6 A_{n1} - 652,1 T_{n1} + 1423,5 A_{n2} + 650,2 T_{n2} + 393,6 A_{n3} + 199,9 T_{n3} + 1120,2 A_{n4} - 216,6 T_{n4} + 1164 A_{n5} + 172,4 T_{n5} - 598,6 A_{n6} - 124,4 T_{n6} \quad (15)$$

The NRMSE for equation (15) yields values of 0.0306 and 0.0772 for the training and testing datasets, respectively. Figure 16 compares the actual and estimated tumor diameters for the training and testing data.

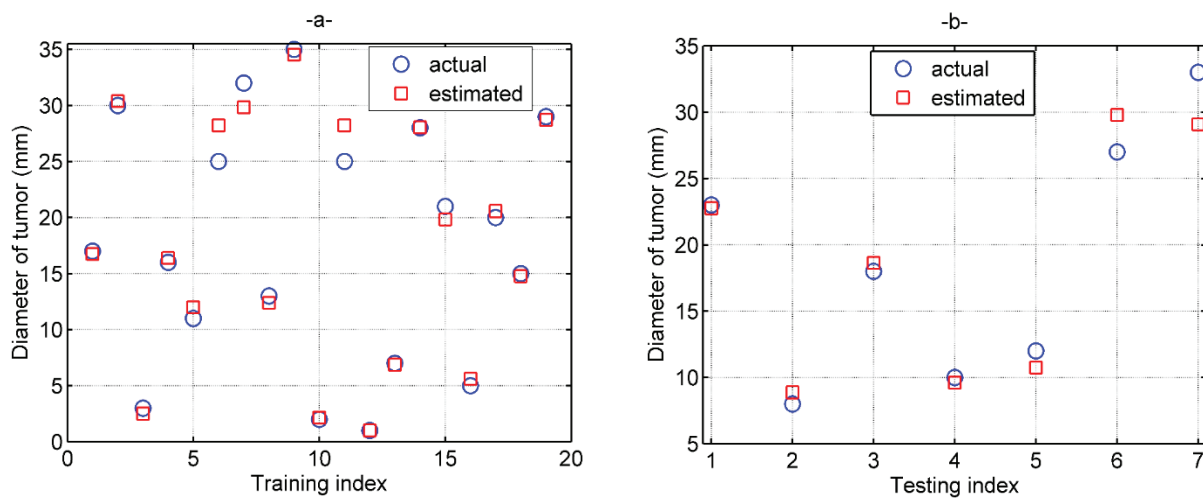


**Figure 16.** Comparison between the actual and estimated diameter of tumor, a) Training, b) Testing.

## CONCLUSIONS

In this study, a microwave imaging system featuring a UWB antenna was developed for the dual purpose of breast cancer detection and tumor diameter estimation. To begin, a UWB antenna structure capable of radiating frequencies from 1 GHz to 12 GHz was constructed and subjected to testing. This antenna offers several advantages, including UWB functionality, compact size, cost-effectiveness, excellent directional radiation patterns with substantial gains (6.76 dBi at 9.8 GHz), and an overall antenna efficiency exceeding 90% across the entire frequency band of 1.6 GHz to 11.2 GHz. Notably, the antenna maintains low Specific Absorption Rate (SAR) values (0.2 W/kg, 2 W/kg) within the safety limits defined by the ICNIRP standard, ensuring safe usage. Next, a human breast model was designed to incorporate tumor diameters spanning from 1 mm to 35 mm, facilitating the detection of breast cancer. Subsequently, this breast model was positioned in front of both the transmitter and receiver antennas, allowing the recording of backscattered waves emitted by the breast model. Simulation results revealed that the highest current density within the breast area adjacent to the tumor reaches 188 A/m<sup>2</sup> for a tumor diameter of 30 mm. In comparison, the lowest recorded current density within the breast in the presence of a tumor is 140 A/m<sup>2</sup> for a tumor diameter of 5 mm. Furthermore, a novel approach utilizing multiple linear regression was applied to the received signals to estimate tumor diameters. The proposed model achieved an impressive accuracy rate of 92.28% for determining the diameter of breast tumors. Importantly, this method offers a less invasive and safer alternative compared to traditional mammography and tomography, which involve high-intensity X-rays for breast cancer detection. Thanks to its wearable design, the proposed system enables early detection of breast cancer tumors, ensuring ease of use for women and

supporting daily usage more effectively than conventional methods.

The findings presented in this study hold applicability solely within the context of the specific model, tumor type, tumor diameter, and tumor location considered. It's important to note that the coefficients of the proposed model may vary when different factors, such as tumor sizes, antenna positions, and the number of tumors, are introduced. In future research endeavors, there is potential for developing a more realistic breast model. Additionally, enhancements could be made to the system to determine tumor diameter and the precise location and quantity of tumors within the breast. Optimized positions for both the receiver and transmitter antennas could be explored for improved performance. Moreover, the proposed system could be physically fabricated to compare experimental results and simulations directly.

## AUTHORSHIP CONTRIBUTIONS

Authors equally contributed to this work.

## DATA AVAILABILITY STATEMENT

The authors confirm that the data that supports the findings of this study are available within the article. Raw data that support the finding of this study are available from the corresponding author, upon reasonable request.

## CONFLICT OF INTEREST

The author declared no potential conflicts of interest with respect to the research, authorship, and/or publication of this article.

## ETHICS

There are no ethical issues with the publication of this manuscript.

## REFERENCES

- [1] Howlader N, Noone AM, Krapcho M, Miller D, Brest A, Yu M, et al. SEER Cancer Statistics Review, 1975-2016, National Cancer Institute. Available at: [https://seer.cancer.gov/csr/1975\\_2016/](https://seer.cancer.gov/csr/1975_2016/). Accessed Oct 6, 2023.
- [2] BCS. Breast Cancer Statistics. Available at: <https://www.wcrf.org/dietandcancer/cancer-trends/breast-cancer-statistics>. Accessed Nov 21, 2022.
- [3] GCO. Global Cancer Observatory. Available at: <https://gco.iarc.fr/#cancer-overtime>. Accessed Nov 21, 2022.
- [4] US BCS. US Breast Cancer Statistics. Available at: <https://www.breastcancer.org/facts-statistics>. Accessed Nov 21, 2022.
- [5] BCF. Breast Cancer Facts. Available at: <https://www.europadonna.org/breast-cancer-facs/>. Accessed Nov 21, 2022.
- [6] Park EH, Min SY, Kim Z, Yoon CS, Jung KW, Nam SJ, et al; Korean Breast Cancer Society. Basic facts of breast cancer in Korea in 2014: The 10-Year overall survival progress. *J Breast Cancer* 2017;20:1–11. [\[CrossRef\]](#)
- [7] Humphrey LL, Helfand M, Chan BK, Woolf SH. Breast cancer screening: A summary of the evidence for the US Preventive Services Task Force. *Ann Intern Med* 2002;137:347–630. [\[CrossRef\]](#)
- [8] Huynh PT, Jarolimek AM, Daye S. The false-negative mammogram. *RadioGraphics* 1998;18:1137–1154. [\[CrossRef\]](#)
- [9] Kornguth PJ, Keefe FJ, Wright KR, Delong DM. Mammography pain in women treated conservatively for breast cancer. *J Pain* 2000;1:268–274. [\[CrossRef\]](#)
- [10] Nass S, Henderson I, Lashof J. Mammography and beyond: Developing technologies for the early detection of breast cancer. 1st ed. Washington: National Academy Press; 2001. [\[CrossRef\]](#)
- [11] Wörtge D, Moll J, Krozer V, Bazrafshan B, Hübner F, Park C, et al. Comparison of X-ray-mammography and planar UWB microwave imaging of the breast: First results from a patient study. *Diagnostics Basel* 2018;8:54. [\[CrossRef\]](#)
- [12] Lehman CD, Isaacs C, Schnall MD, Pisano ED, Ascher SM, Weatherall PT, et al. Cancer yield of mammography, MR, and US in high-risk women: Prospective multi-institution breast cancer screening study. *Radiology* 2007;244:381–388. [\[CrossRef\]](#)
- [13] Wang J, Chen H, Wu X, Tang L. Comparison of diagnostic efficiency of breast cancer imaging in Chinese women: Digital mammography, Ultrasound, MRI, and combinations of these modalities. *J Med Imaging Health Inform* 2015;5:1488–1493. [\[CrossRef\]](#)
- [14] Kwon S, Lee S. Recent advances in microwave imaging for breast cancer detection. *Int J Biomed Imaging* 2018;2018:1657073. [\[CrossRef\]](#)
- [15] Kriege M, Brekelmans CT, Boetes C, Besnard PE, Zonderland HM, Obdeijn IM, et al. Efficacy of MRI and mammography for breast-cancer screening in women with a familial or genetic predisposition. *N Engl J Med* 2004;351:427–437. [\[CrossRef\]](#)
- [16] Stuchly MA, Fear EC. Microwave detection of breast cancer. *IEEE Trans Microw Theory Techn* 2000;48:1854–1863. [\[CrossRef\]](#)
- [17] Nikolova NK. Microwave imaging for breast cancer. *IEEE Microwave Magazine*. 2011;12:78–94. [\[CrossRef\]](#)
- [18] Zhang H. Microwave imaging for ultra-wideband antenna-based cancer detection. Edinburgh: The University of Edinburgh; 2015.
- [19] Mahmud MZ, Islam MT, Misran N, Almutairi AF, Cho M. Ultra-wideband (UWB) antenna sensor based microwave breast imaging: A review. *Sensors* 2018;18:2951. [\[CrossRef\]](#)
- [20] Wang L. Microwave sensors for breast cancer detection. *Sensors* 2018;18:655. [\[CrossRef\]](#)
- [21] Mukherjee S, Su Z, Udpa L, Udpa S, Tamburrino A. Enhancement of microwave imaging using a metamaterial lens. *IEEE Sensors J* 2019;19:4962–4971. [\[CrossRef\]](#)
- [22] Lazebnik M, Popovic D, McCartney L, Watkins CB, Lindstrom MJ, Harter J, et al. Large scale study of the ultrawideband microwave dielectric properties of normal, benign, and malignant breast tissues obtained from cancer surgeries. *Phys Med Biol* 2007;52:6093–6115. [\[CrossRef\]](#)
- [23] Al Ahmad MZ, Natour Z, Mustafa F, Rizvi TA. Electrical characterization of normal and cancer cells. *IEEE Access* 2018;6:25979–25986. [\[CrossRef\]](#)
- [24] De S, Biswas P, Sarkar S, Biswas S, Sarkar D, Sarkar PP. Novel method for detection of breast cancer or tumor. *Int J Electron Commun Technol* 2016;7:12–14.
- [25] Cheng Y, Fu M. Dielectric properties for non-invasive detection of normal, benign, and malignant breast tissues using microwave theories. *Thoracic Cancer* 2018;9:459–465. [\[CrossRef\]](#)
- [26] Rossi S, Garbagnati F, Lencioni R, Allgaier HP, Marchianò A, Fornari F, et al. Percutaneous radiofrequency thermal ablation of nonresectable hepatocellular carcinoma after occlusion of tumor blood supply. *Radiology* 2000;217:119–126. [\[CrossRef\]](#)
- [27] FCC. Revision of part 15 of the commission's rules regarding ultra-wideband transmission systems. *Tech Rep FCC* 2002;02:48.
- [28] Fouad S, Ghoname R, Elmahdy A, Zekry A. Enhancing tumor detection in IR-UWB breast cancer system. *Int Sch Res Notices* 2017;4606580. [\[CrossRef\]](#)
- [29] Khan MM, Shanaz S, Al-Mamun A. Investigation of performance parameters of different wearable narrowband antennas in close proximity to the human body, 15th International Conference on Computer and Information Technology, 22-24 December, Chittagong, Bangladesh, 2012. [\[CrossRef\]](#)

- [30] Koutsoupidou M, Karanasiou I, Kakoyiannis C, Groumpas E, Conessa C, Joachimowicz N, et al. Evaluation of a tumor detection microwave system with a realistic breast phantom. *Microwave Opt Technol Lett* 2017;59:6–10. [CrossRef]
- [31] Ouerghi K, Fadlallah N, Smda A, Ghayoula R. Circular Antenna Array Design for Breast Cancer Detection, *Sensors Networks Smart and Emerging Technologies (SENSET)*, 12-14 September, Beirut, Lebanon, 2017. [CrossRef]
- [32] Rahman A, Aziz A, Ahmad Dhruho, Shila TA. On-Body Circular Patch Antenna for Breast Cancer Detection, *IEEE International Electromagnetics and Antenna Conference*, 17-19 October, Vancouver, Canada, 2019.
- [33] Chiappe M, Gragnani GL. Vivaldi antennas for microwave imaging: Theoretical analysis and design considerations. *IEEE Trans Instrumentation Measurement* 2006;55:1885–1891. [CrossRef]
- [34] Zhang J, Fear EC, Johnston RH. Cross-Vivaldi antenna for breast tumor detection. *Microwave Opt Technol Lett* 2009;51:275–280. [CrossRef]
- [35] Jalilvand M, Vasaneli C, Wu C, Kowalewski J. On the evaluation of a proposed bowtie antenna for microwave tomography, *The 8th European Conference on Antennas and Propagation (EuCAP 2014)*, 6-11 April, The Hague, Netherlands, 2014. [CrossRef]
- [36] Shrestha S, Agarwal M, Reid J, Varahramyan K. Microstrip Antennas for Direct Human Skin placement for Biomedical Applications, *PIERS Proceedings*, Cambridge, USA.
- [37] Sharma MK, Kumar M, Saini PS, Gangwar D. Experimental investigation of the breast phantom for tumor detection using ultra-wide band-MIMO antenna sensor (UMAS) probe. *IEEE Sensors Journal* 2020;20:6745–6752. [CrossRef]
- [38] Islam MT, Mahmud Z, Misran N, Takada J, Cho M. Microwave breast phantom measurement system with compact side slotted directional antenna. *IEEE Access* 2017;5:5321–5330. [CrossRef]
- [39] Zhang H. Microwave imaging for breast cancer detection: The discrimination of breast lesion morphology. *IEEE Access* 2020;8:107103–107111. [CrossRef]
- [40] Kwon S, Lee H, Lee S. Image enhancement with Gaussian filtering in time-domain microwave imaging system for breast cancer detection. *Electronics Letters* 2016;52:342–344. [CrossRef]
- [41] Subramanian S, Sundarambal B, Nirmal D. Investigation on simulation-based specific absorption rate in ultra-wideband antenna for breast cancer detection. *IEEE Sensors J* 2018;18:10002–10009. [CrossRef]
- [42] Misilmani HME, Naous T, Khatib SA, Kaban KY. A survey on antenna designs for breast cancer detection using microwave imaging. *IEEE Access* 2020;8:102570–102594. [CrossRef]
- [43] Hammouch N, Ammor H. Microwave Imaging for Early Breast Cancer Detection using CMI, *7th Mediterranean Congress of Telecommunications (CMT)*, Fès, Morocco, 2019. [CrossRef]
- [44] Rahayu Y, Hilmi MF, Masdar H. A Novel Design Rectangular UWB Antenna Array for Microwave Breast Tumor Detection, *16th International Conference on Quality in Research (QIR) - International Symposium on Electrical and Computer Engineering*, Padang, Indonesia, 2019. [CrossRef]
- [45] Alsharif F, Kurnaz Ç. Wearable Microstrip Patch Ultra-Wide Band Antenna for Breast Cancer Detection, *41st International Conference on Telecommunications and Signal Processing (TSP)*, 4-6 July, Athens, Greece, 2018. [CrossRef]
- [46] Alsharif F, Kurnaz Ç. Evaluation of Non-Wearable Antennas and Wearable Ultra-Wideband Antenna Used in Microwave Imaging for Breast Cancer Detection, *7th International Conference on Advanced Technologies*, 28 April - 1 May, Antalya, Türkiye, 2018.
- [47] Alsharif F, Kurnaz Ç. Wearable Microstrip Ultra-Wideband Antenna used for Early Breast Cancer Detection. *7th International Conference on Advanced Technologies*, 28 April-1 May, Antalya, Türkiye, 2018. [CrossRef]
- [48] Bidhendi H, Jafari H, Genov R. Ultra-Wideband Imaging Systems for Breast Cancer Detection, In: Yuce M, editor. *Ultra-Wideband and 60 GHz Communications for Biomedical Applications*. Boston: Springer; 2014. [CrossRef]
- [49] Joines WT, Zhang Y, Li C, Jirtle RL. The measured electrical properties of normal and malignant human tissues from 50 to 900 MHz. *Med Phys* 1994;21:547–550. [CrossRef]
- [50] Gabriel C, Gabriel S, Corthout E. The dielectric properties of biological tissues: I. Literature survey. *Phys Med Biol* 1996;41:223. [CrossRef]
- [51] Balanis CA. *Antenna theory, analysis and design*. 4th ed. New Jersey: Wiley; 2016.
- [52] Bhartia P, Bahl I, Garg R, Ittipiboon A. *Microstrip Antenna Design Handbook*. Norwood: Artech House; 2000.
- [53] Kumar G, Ray KP. *Broadband Microstrip Antennas*. Dedham: Artech House; 2003.
- [54] Alsharif F, Safi S, Aboufoul T, Nasr MA. Mechanical reconfigurable microstrip antenna. *Int J Microwave Opt Technol* 2016;11:153–160.
- [55] Byrne D, Sarafiano M, Craddock I. Compound radar approach for breast imaging. *IEEE Trans Biomed Eng* 2017;64:40–51. [CrossRef]
- [56] CST. *Computer Simulation Technology Studio Suite*. Available at: <https://www.3ds.com/products-services/simulia/products/cst-studio-suite/>. Accessed Nov 21, 2022.

- 
- [57] Hammouch N, Ammor H. An accurate UWB technique for breast cancer detection using microwave specific absorption rate. *Int J Microwave Opt Technol* 2018;13:424–431.
- [58] IEEE. IEEE Std. C95.3.1. IEEE Recommended Practice for Measurements and Computations of Radio Frequency Electromagnetic Fields with Respect to Human Exposure to Such Fields, 100 kHz-300 GHz. Available at: [https://www.sandiegocounty.gov/content/dam/sdc/pds/ceqa/Soitec-Documents/Final-EIR-Files/references/rtcref/ch9.0/RTCrefappx/2014-12-19\\_IEEE2010.pdf](https://www.sandiegocounty.gov/content/dam/sdc/pds/ceqa/Soitec-Documents/Final-EIR-Files/references/rtcref/ch9.0/RTCrefappx/2014-12-19_IEEE2010.pdf). Accessed Oct 6, 2023.
- [59] ICNIRP. Guidelines for limiting exposure to time-varying electric, magnetic and electromagnetic fields (up to 300 ghz). *Health Phys* 1998;74:494–522.
- [60] ACS. American Cancer Society. Available at: <https://www.cancer.org/cancer/breast-cancer/screening-tests-and-early-detection.html>. Accessed Nov 21, 2022.